


# Graph Theoretical Analysis of Organization of Functional Brain Networks in ADHD

Clinical EEG and Neuroscience  
43(1) 5-13  
© EEG and Clinical Neuroscience  
Society (ECNS) 2012  
Reprints and permission:  
sagepub.com/journalsPermissions.nav  
DOI: 10.1177/1550059411428555  
http://eeg.sagepub.com  


Mehran Ahmadi<sup>1</sup>, Hojjat Adeli<sup>2</sup>, and Amir Adeli<sup>3</sup>

## Abstract

This article presents a new methodology for investigation of the organization of the overall and hemispheric brain network of patients with attention-deficit hyperactivity disorder (ADHD) using theoretical analysis of a weighted graph with the goal of discovering how the brain topology is affected in such patients. The synchronization measure used is the nonlinear fuzzy synchronization likelihood (FSL) developed by the authors recently. Recent evidence indicates a normal neocortex has a small-world (SW) network with a balance between local structure and global structure characteristics. Such a network results in optimal balance between segregation and integration which is essential for high synchronizability and fast information transmission in a complex network. The SW network is characterized by the coexistence of dense clustering of connections ( $C$ ) and short path lengths ( $L$ ) among the network units. The results of investigation of  $C$  show the local structure of functional left-hemisphere brain networks of ADHD diverges from that of non-ADHD which is recognizable in the delta electroencephalograph (EEG) sub-band. Also, the results of investigation for  $L$  show the global structure of functional left-hemisphere brain networks of ADHD diverges from that of non-ADHD which is observable in the delta EEG sub-band. It is concluded that the changes in left-hemisphere brain's structure of ADHD from that of the non-ADHD are so much that  $L$  and  $C$  can distinguish the ADHD brain from the non-ADHD brain in the delta EEG sub-band.

## Keywords

Attention-deficit hyperactivity disorder, Electroencephalogram, small-world network, synchronization

Received May 30, 2011; accepted August 6, 2011.

## Introduction

Many neuroanatomical and neuropsychological studies have shown that patients with attention-deficit hyperactivity disorder (ADHD) have structurally abnormal brains. In comparison with healthy participants, studies have reported significantly smaller brain volume<sup>1,2</sup>; smaller bifrontal cortex volumes<sup>3</sup>; smaller basal ganglia<sup>4</sup>; and a smaller cerebellum.<sup>5-7</sup> Plessen et al<sup>8</sup> reported abnormal connectivity between the amygdala and prefrontal cortex. There are also reports of other specific deficits in ADHD's brain structure, such as smaller dorsolateral prefrontal, caudate, putamen, right and left globus pallidus, anterior frontal regions, and corpus callosum.<sup>4-6,9</sup> All the aforementioned have taken advantages of magnetic resonance imaging (MRI)<sup>10</sup> to determine discriminative structural brain abnormalities of ADHD.

Many articles have been published on EEG-based investigation of neurological disorders, in particular epilepsy and more recently in Alzheimer's disease.<sup>11-24</sup> There are few studies on EEG-based investigation of structural brain abnormalities of ADHD, and all of them deal only with local (locus to locus or area to area) neuronal connectivity deficits in ADHD. The

studies have estimated synchronizations between EEG signals.<sup>25-31</sup> Measurements of synchronizations between different EEG signals have quantified interdependencies and functional interactions between the related neuronal areas.<sup>32</sup> Before the authors' recent research, all EEG-based studies of ADHD used *linear synchronization measurement methods* to demonstrate the connectivity deficits in a specific task or in a resting state, and in certain EEG sub-bands or

<sup>1</sup> Department of Biomedical Engineering, Amirkabir University of Technology, Tehran, Iran

<sup>2</sup> Departments of Biomedical Engineering, Biomedical Informatics, Civil and Environmental Engineering and Geodetic Science, Electrical and Computer Engineering, Neurological Surgery, and Neuroscience, Ohio State University, Columbus, OH, USA

<sup>3</sup> Department of Neurology, Ohio State University, Columbus, OH, USA

## Corresponding Author:

Hojjat Adeli, Departments of Biomedical Engineering, Biomedical Informatics, Civil and Environmental Engineering and Geodetic Science, Electrical and Computer Engineering, Neurological Surgery, and Neuroscience, 470 Hitchcock Hall, 2070 Neil Avenue, Ohio State University, Columbus, Ohio 43210, USA

Email: adeli.h@osu.edu

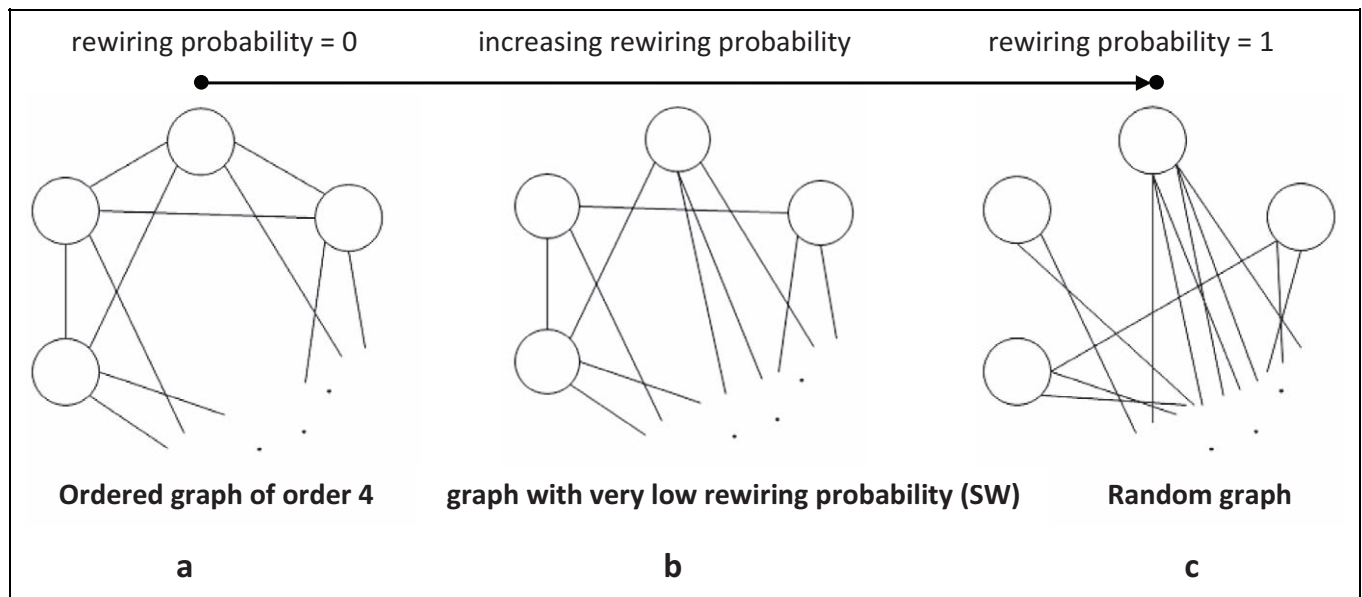


**Figure 1.** A, A simple configuration of an ordered graph. B, An SW graph. C, A random graph. SW graph is a graph with very low rewiring probability (near 0). Whereas rewiring probabilities of an ordered graph and a random graph are 0 and 1, respectively. SW indicates small world.

in the entire band-limited EEG. Recently, the authors presented a multiparadigm methodology for EEG-based diagnosis of ADHD through adroit integration of nonlinear science,<sup>33</sup> wavelets,<sup>34–37</sup> and neural networks<sup>38</sup> following the senior author's research on epilepsy<sup>39–45</sup> and Alzheimer's disease.<sup>46–49</sup> The general methodology is based on identification of nonlinear features known as **synchronization likelihoods (SLs)**,<sup>50</sup> both among all electrodes and among electrode pairs. The methodology was applied to EEG data obtained from 47 ADHD and 7 control individuals with eyes closed. Based on the analysis of variance (ANOVA) statistical test, the methodology yielded a **high accuracy of 96.5% for diagnosis of ADHD**. To the best of the authors' knowledge that was the first study of ADHD brain connectivity deficits based on **nonlinear science**.

All of the aforementioned studies, using MRI measurements or EEG analyses, confirm the existence of **structural abnormalities in the brains of the patients with ADHD but report a diversity of abnormalities**. The differences between the reported abnormal neuronal connectivity and local dysfunctions are possibly due to a diversity of the ADHD as well as overlap with other disorders exhibiting similar symptoms such as learning disorder (LD) and mood disorders.

The optimum structure of a network is the one that has a balance between local and global structural characteristics which lead to an appropriate optimal balance between segregation and integration. Modern networks theory calls a network with a structure near such optimum structure "small-world (SW) network."<sup>51–55</sup> It is characterized by the coexistence of dense clustering of connections and short path lengths ( $L$ ) among the network units. In the SW network, the highest synchronizability and the highest speed of information transition

among the network functional units exist compared with other types of network structures such as random, lattice, and ordered networks. **Recent research indicates normal neocortex and different areas in brain may have SW structures.**<sup>52,53</sup>

To the best of the authors' knowledge there is no EEG-based, electromyography (EMG)-based, or imaging-based study on organization of the functional brain networks in the ADHD brain, which may reveal common discriminative characteristics in all patients with ADHD. From a physiological perspective, a recorded brain EEG is commonly divided into 5 sub-bands: **delta (0–4 Hz), theta (4–8 Hz), alpha (8–12 Hz), beta (13–30 Hz), and gamma (30–60 Hz)**. This article presents a new methodology for the investigation of the organization of the overall and hemispheric brain network of patients with ADHD using theoretical analysis of a weighted graph, with the goal of discovering how the topology of overall and hemispheric brain functional connectivity networks are affected in such patients in **full-band EEG** as well as the 5 aforementioned EEG sub-bands.

## Graph Theoretical Analysis

Graph theoretical analysis (GTA) has been used as a useful and efficient tool for the investigation of SW and other network topologies.<sup>56–58</sup> In GTA, the network functional units and the connections between them are modeled as vertexes and edges, respectively. Figure 1A shows an ordered graph whose nodes connect to the same number of edges (e.g. 4 edges in Figure 1A). When the edges are rewired slightly (ie, disconnecting an edge from one of the nodes and connecting to another node), the network will change to a SW graph shown in Figure 1B. In this view, an entirely random graph is a graph with completely random rewiring (Figure 1C).

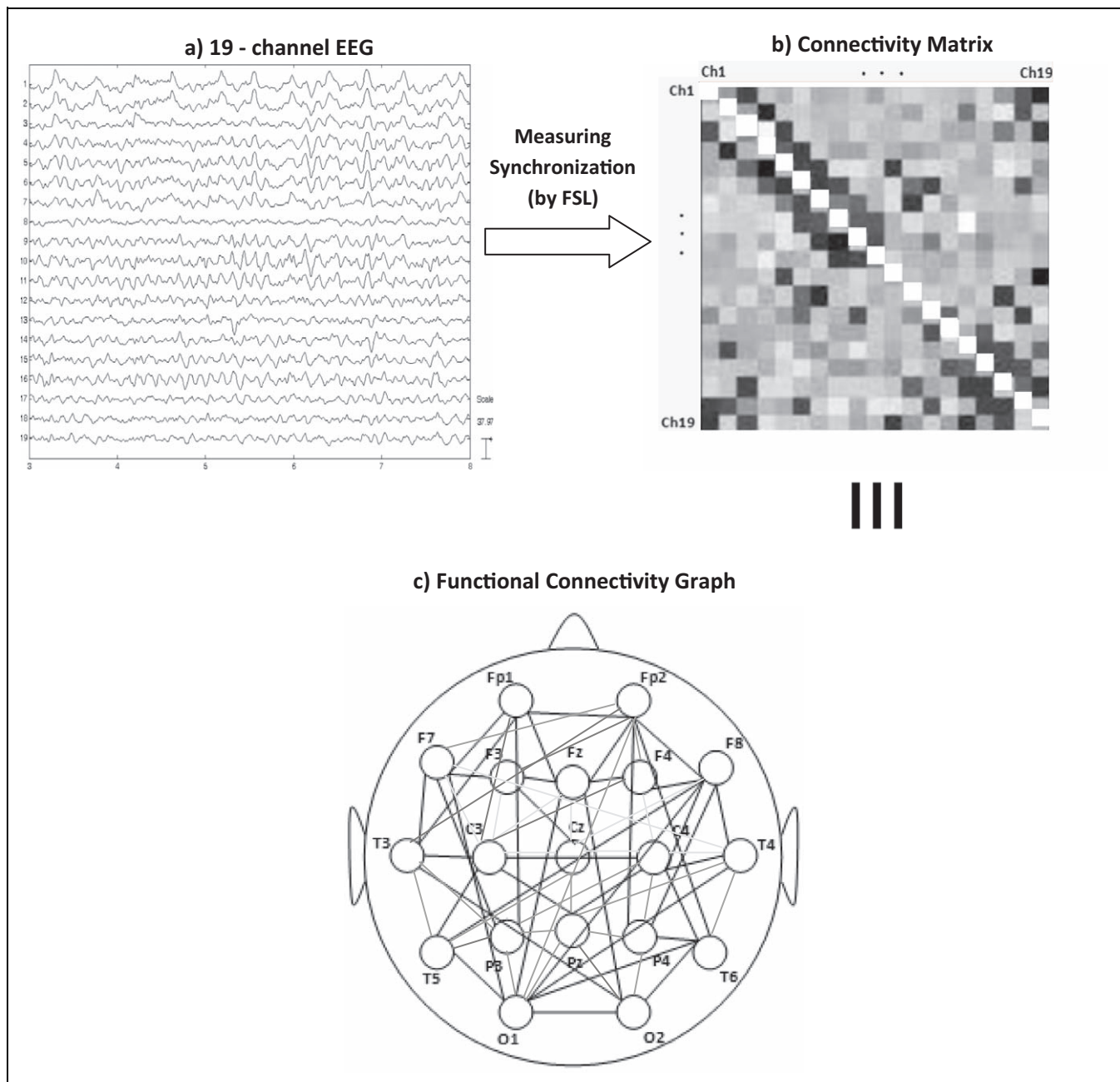


**Figure 2.** Illustration of procedure for transforming a 19-channel EEG to its connectivity graph. EEG indicates electroencephalograph.

Figure 2 shows how an example of a 19-channel digital EEG set (Figure 2A) is transformed to its connectivity graph shown in Figure 2C. Computed synchronization values between channel pairs are placed in the arrays (squares) of a  $19 \times 19$  connectivity matrix (Figure 2B). The light color of each array indicates the strength of the connectivity. The darker color indicates a larger value in the connectivity matrix, which corresponds to a darker edge in the corresponding functional connectivity graph (Figure 2C).

Major characteristics of a weighted graph, as the model of a complex network topology, are clustering coefficient ( $C$ ) as an indicator of the local structure and  $L$  as an indicator of the

global structure of the network. Small-world network has a high  $C$  value ( $C$  varies from 0 to 1), a value close to 1, and a low  $L$  value ( $L$  varies from 0 to number of nodes in the graph), a number substantially less than the number of nodes. On the contrary, a random network has a much lower value of  $C$  (close to 0) and a lower value of  $L$  simultaneously, and regular networks have larger values of  $C$  (close to 1) and  $L$  simultaneously.<sup>51,59,60</sup> This means random and regular networks do not have a balance between synchronizability and speed of information transition or a balance between segregation and integration.

The first application of GTA to the EEG-based investigation appears to have been reported by Stam et al.<sup>61</sup> on Alzheimer's

disease. In the following year, Liu et al.<sup>54</sup> studied functional MRI of schizophrenia through GTA. In both studies, researchers report disruption of the SW topology of the brain and changes in the brain network configuration.

## Methodology

In the authors' previous research, using wavelet decomposition, SL was computed for all different EEG sub-bands and the entire EEG, and significantly discriminative SLs in distinguishing children with ADHD from non-ADHD children were discovered.<sup>38</sup> Recently, the authors presented a new measure of synchronization, **fuzzy SL (FSL)**, using the theory of **fuzzy logic and Gaussian membership functions** and showed that it is more reliable than SL for **measuring the interdependencies especially in weak couplings**. The results of ANOVA indicate the interdependencies measured by FSL are more reliable than the conventional SL for discriminating patients with ADHD from healthy individuals.<sup>62</sup>

In this study, the connectivity and interdependencies of each electrode pair to be used in **connectivity matrices of GTA are obtained using their bivariate FSL**. Following the **wavelet-chaos** approach of Adeli et al.,<sup>39,40</sup> **since the discriminative nonlinear features, FSLs, may represent themselves in certain sub-bands and not necessarily in the entire band-limited EEG, the band-limited EEG is divided into its 5 sub-bands through a wavelet filter bank**.

There is some evidence for interdependencies of long and short distance areas of the brain which affect the synchronization of EEGs in different frequency sub-bands (short-distance synchronization mostly occurs at high-frequency EEG sub-bands, and low-frequency EEG sub-bands are related to long-distance synchronization).<sup>62,63</sup> As such, the functional connectivity matrices containing FSLs are computed for each sub-band and for the entire band-limited EEG. Then, C and L of the graphs corresponding to overall brain and left and right hemispheres are computed. Using the 1-way ANOVA statistical test, meaningful C and L to differentiate ADHD from non-ADHD brains are discovered. The methodology consists of 5 steps as follows.

### Step 1: Preprocessing and Wavelet Decomposition

Details of this step can be found in Ahmadlou and Adeli<sup>38</sup> where a block diagram of the data preprocessing and wavelet analysis is presented. An infinite impulse response (IIR) low pass filter is applied to obtain a band-limited EEG in the range of 0 to 60 Hz range. Following Adeli et al.,<sup>40</sup> using a 4-level wavelet decomposition, **the EEG is divided into 5 sub-bands: gamma (30-60 Hz), beta (15-30 Hz), alpha (8-15 Hz), theta (4-8 Hz), and delta (0-4 Hz)**.

### Step 2: Computing Bivariate FSLs

In contrast to linear synchronization measurements such as coherence and cross correlation, FSL is an unbiased

measurement of both linear and nonlinear synchronizations among 2 or more coupled systems. Fuzzy SL is used as a bivariate measurement, which quantifies likelihood and similarity between dynamics of signals of each electrode pair. Fuzzy SL measures the **similarity of reconstructed trajectories from the signals**. The trajectories are reconstructed in a state space according to Taken's theorem by determining 2 characteristics: embedding and the lag dimensions. Fuzzy SL varies from 0 (for independent systems) to 1 (for completely synchronous systems). Computation of bivariate FSL is presented in Appendix A.

### Step 3: Creating Connectivity Matrices

In this step, the connectivity matrices are created with values of the FSL between signals of all pairwise combinations of the channels (obtained in the previous step) as well as all pairwise combinations of the channels in left and right hemispheres of the brain separately. As such, 3 connectivity matrices are calculated for each EEG sub-band and for the entire band-limited EEG. Therefore, each patient has 18 (3 [right hemispheric, left hemispheric, and overall brain]  $\times$  6 [1 band-limited EEG and 5 EEG sub-bands]) connectivity matrices.

### Step 4: Graph Theoretical Analysis

A **bidirectional weighted graph** is used in this study. A weighted graph is defined by an adjacency matrix of values between 0 and 1, which shows the strengths of the connections between the corresponding nodes. The term "bidirectional" means an edge between nodes has no direction. Adjacency matrix of a bidirectional weighted graph is a symmetric matrix as shown in the example of Figure 2B. **Since the bivariate FSL does not show which node (EEG locus) is the driver and which one is the responder, the relationship is bidirectional**. The connectivity matrices obtained from the previous step are not binary (they include values between 0 and 1). It has been shown that the weights of the connections preserve essential information of a network structure.<sup>60,65,66</sup> Hence the weighted graphs are used directly for the analysis in this study.

Figure 3A shows a fully connected triple-node graph. Figure 3B shows a triple-node graph with only 2 edges. Nodes have been numbered 1, 2, and 3 and  $a_{ij}$  indicates a connection between node  $i$  and node  $j$ . If 1 connection in a fully interconnected triple node (see Figure 3a) is removed, information can still be transferred among the 3 nodes through the remaining edges. In contrast, if 3 nodes are not fully connected together (see Figure 3B), removing 1 edge ( $a_{12}$  or  $a_{31}$ ) completely disconnects a node (node 2 or node 3) from the other 2 nodes. Figure 3C shows information from node 1 or 3 cannot be transferred to node 2. **The shortest path length of a graph ( $L$ ) is an average of the shortest path that exists between each node pairs for all node pairs and conceptually demonstrates the speed of information transmission among nodes.**



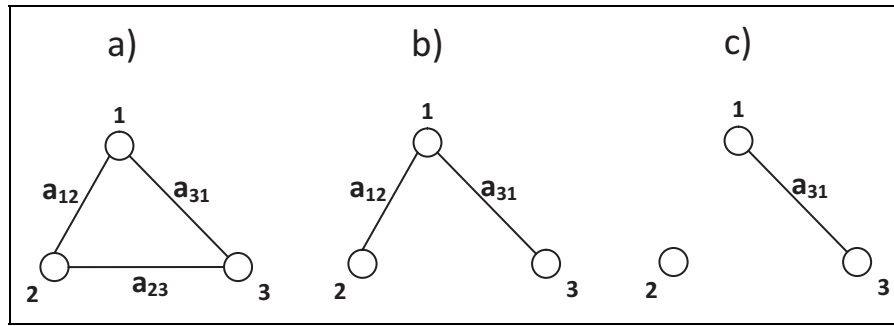


**Figure 3.** Illustration of 2 different types of triple-node graphs: (A) a fully connected graph; (B) a nonfully connected graph; (C) nonfully connected graph of (B) without edge  $a_{12}$ .

In this work, the clustering coefficient is defined in term of the connectivity of triple-node graphs and computed as follows<sup>60</sup>:

$$C = \frac{1}{N} \sum_{i=1}^N \frac{\sum_{1 \leq j < k \leq N} a_{ij} a_{jk} a_{ki}}{\sum_{1 \leq j < k \leq N} a_{ij} a_{ik}} \quad (1)$$

Where  $a_{ij}$  is the weight of the edge connecting the  $i$ th node to the  $j$ th node, and  $N$  is the number of nodes in the graph. Indeed,  $C$ , varying between 0 and 1, represents redundancy and quantifies how strongly the information is transmitted in the graph when some connections are disturbed (such as in the case of a brain disorder when neurons or neuronal areas do not function properly or their connections are dead). The clustering coefficient  $C$  is defined to measure the robustness of the brain network information transmission performance. A high value of  $C$  means existence of a large number of fully interconnected triple nodes and high robustness. Since  $C$  is defined in term of the local units (triple nodes), it is known as a local quantification parameter, but it also represents the global organization of the network because it demonstrates how much of all pairwise combinations of neighbors of each vertex (node) are connected together. Indeed it shows what portion of all triple combinations of nodes is fully connected.

$L$  is inversely related to the speed of information transmission in the graph and is considered a global quantification measure. It is computed as follows<sup>66,67</sup>:

$$L = \frac{1}{N(N-1)/2} \sum_{1 \leq j < i \leq N} \left( \frac{1}{d_{ij}} \right) \quad (2)$$

where  $d_{ij} = \frac{1}{a_{ij}}$  is defined as the inverse of the weight between  $i$ th and  $j$ th nodes.

### Step 5: Analysis of Variance Test

The 1-way ANOVA is a statistical test that demonstrates how strongly a feature can distinguish a class from another class by a value, called  $P$  value, which varies between 0 and 1; where a  $P$  value near 0 shows the high ability of the feature in discriminating the groups and a  $P$  value close to 1 indicates high similarity of distribution and closeness of the groups. The

1-way ANOVA statistical test is used for evaluation of  $C$  and  $L$  in terms of distinguishing the ADHD group from the non-ADHD group. A  $P$  value of .05 is considered as the threshold for showing significant difference between the groups in each hemisphere and in the overall brain in the sub-bands studied (delta, theta, alpha, beta, and gamma).

### Data Acquisition

The EEG data were collected from 12 patients with ADHD (8-13 years old; 3 girls and 9 boys) and 12 control individuals (8-13 years old; 3 girls and 9 boys), with eyes closed and resting. Parents of the patients provided informed consent. The ADHD group includes all clinical subtypes (hyperactive impulsive, inattentive, and combined). Scalp electrodes were applied according to the International 10-20 System and all data were recorded with a sampling rate of 256 Hz digitized by 16 digits. The EEG recording lasted 3 minutes ( $3 \times 60 \times 256 = 46\,080$  time samples) in order to have a large interval free from artifacts. Data for each patient or control participant consist of 19 channels and as such a total of  $19 (12 + 12) = 456$  EEGs was obtained from 24 participants. For additional information on data collection, see Ahmadlou and Adeli.<sup>38</sup>

### Results

After passing a 50 Hz notch filter (for removing the line electricity noise) and a 60 Hz low pass filter and applying the wavelet decomposition to the EEGs in 4 levels, 5 EEG (gamma, beta, alpha, theta, and delta) sub-bands and 1 band-limited EEG were obtained from EEG of each individual, resulting in a total of  $(5 + 1; \text{number of EEG sub-bands} + 1 \text{ band-limited EEG}) \times 19 (\text{number of channels}) = 114$  signals for each participant.

Based on these values, the state space was determined and the trajectories of the EEG channels were reconstructed. The embedding and the lag dimensions were chosen equal to 12 and 5, respectively, determined to be large enough to avoid folding in the trajectories, which is needed for computation of FSL.<sup>62</sup> Then, the bivariate FSL of each channel pair was computed for each EEG sub-band and the band limited EEGs for all  $\frac{19 \times 18}{2} = 171$  (number of combinations of 2 channels from 19

channels) channel pairs. Therefore, six  $19 \times 19$  overall brain connectivity matrices were computed for each participant ( $6 = \text{number of EEG sub-bands} + 1 \text{ band-limited EEG}$ ; and  $19 = \text{number of channels}$ ). Also, six  $8 \times 8$  ( $8 = \text{number of channels in a hemisphere}$ ) hemispheric brain connectivity matrices were computed for each hemisphere and for each participant.

The ANOVA test was used for evaluation of  $C$  and  $L$  in terms of distinguishing the ADHD group from the non-ADHD group. Among all EEG sub-bands and the full-band EEG, and among right and left-hemispheric and overall brain networks, just the  $C$  and  $L$  of left-hemispheric brain network at delta sub-band showed statistically significant differences between ADHD and non-ADHD groups. In low-frequency sub-bands (delta) smaller values of  $L$  (non-ADHD: 5.87 and ADHD: 5.36) and larger values of  $C$  (non-ADHD: 0.078 and ADHD: 0.088) were observed for the ADHD group compared with the non-ADHD group, with  $P$  values of .012 and .037, respectively.

## Conclusion

In recent articles, authors discovered meaningful functional connectivity deficits at low frequencies (theta and delta bands) in ADHD's neocortex based on EEG analysis and using 2 different generalized synchronization methods called synchronization likelihood (SL) and fuzzy synchronization likelihood (FSL).<sup>38,62</sup> This finding raised the question of how much the functional connectivity deficits affect the organization of the functional structure of ADHD's neocortex. This article is an attempt to answer this question. To the best of the authors' knowledge, this article is the first investigation of organization of the ADHD brain network with the goal of discovering how the SW brain topology is affected in patients with ADHD.

In the present study, using wavelet analysis the EEGs of ADHD and non-ADHD children were decomposed to 5 physiological sub-bands and the connectivity matrices were computed using bivariate FSL for the full-band EEG and all EEG sub-bands. Then  $C$  and  $L$  of each graph are computed for overall brain network and hemispheric brain networks to reveal changes in the ADHD's neocortex structure compared with non-ADHD's neocortex structure. This study revealed integration is increased and segregation is decreased in low-frequency sub-band (delta) significantly in ADHD's left-hemispheric neocortex compared with non-ADHD's left-hemispheric neocortex ( $P$  value  $< .05$ ).

The results of investigation of  $C$  and  $L$  show the local and global structures of functional left-hemispheric brain networks of ADHD diverge from that of non-ADHD which is recognizable in delta EEG sub-band. The findings show more abnormality in the structure of the low-frequency (delta) graph which is related to networks of long-distance connectivity<sup>63</sup> in the left hemisphere of ADHD's brain. The deficits found in the left-hemispheric structure may be related to reduced regional gray matter mostly in the left hemisphere of ADHD's brain<sup>68</sup> and

may imply reduced left hemisphere involvement of patients with ADHD in linguistic processing.<sup>69</sup>

In summary, it is concluded that the changes in ADHD left-hemispheric brain's structure when compared to the non-ADHD left-hemispheric brain's structure at delta band are so much that  $L$  and  $C$  can distinguish the ADHD brain from the non-ADHD brain. Although there are **diverse and different changes** in the ADHD brain's structure in different patients (found mostly by imaging techniques), as a diagnostic tool all structural changes can be unified through the detection of  $C$  and  $L$  changes in EEG without using expensive imaging technologies.

## Appendix A

### Computation of Bivariate FSL

Suppose signals  $x_k$  and  $x_r$  are signals of 2 different electrodes,  $k$  and  $r$  (a band-limited electroencephalograph [EEG] or an EEG sub-band). They are reconstructed as trajectories  $X_k$  and  $X_r$  in a state space. According to Taken's method of reconstruction,<sup>70</sup> the  $n$ 'th point of  $X_k$  and  $X_{k,n}$  is represented in the form  $X_{k,n} = (x_{k,n}, x_{k,n+\tau}, \dots, x_{k,n+(d-1)\tau})$  where  $x_{k,n}$  is the  $n$ th sample of the time series  $x_k$ ; and  $d$  and  $\tau$  are time lag and embedding dimension of the state space, respectively. The parameters  $d$  and  $\tau$  are computed so that the reconstructed trajectories have no folding and self-intersection to avoid incorrectly considered close points of the trajectories which can hamper the computation of closeness in the FSL method. Also, both parameters are assumed to have the same value for all signals in order to compute similarities among the trajectories in the same state space for meaningful comparisons.<sup>71,72</sup> Consequently, the number of points of a trajectory ( $N$ ) is equal to  $M - (d - 1)\tau$ ; where  $M$  is the number of sampling points of the signal. A window, around the reference state,  $X_{k,n}$ , contains all states,  $X_{k,m}$ , whose  $m$  indices satisfy the condition  $w_1 < |n - m| < w_2$ . The term  $w_1$  is the Theiler correction<sup>70</sup> used to prevent information redundancy in the similarity computation. Therefore,  $2(w_2 - w_1)$  is the number of points restricted in the window and  $w_2$  determines the maximum temporal distance that a state can have from the reference state.

In the window,  $W_{w_1}^{w_2}(k, n)$ , a Gaussian membership function with center at the reference state and a standard deviation of  $\epsilon_{k,n}$  is employed<sup>62</sup>:

$$\mu_{k,n}(X_{k,m}) = \exp\left(-\frac{|X_{k,m} - X_{k,n}|^2}{\epsilon_{k,n}}\right) \quad (\text{A1})$$

where  $\mu_{k,n}(X_{k,m})$  is the membership value of the state  $X_{k,m}$  in the  $d$  dimensional Gaussian function of the time series  $k$  in the window and  $|X_{k,m} - X_{k,n}|$  indicates the Euclidean distance between the states  $X_{k,m}$  and  $X_{k,n}$ . Then, the probability that a state  $X_{k,m}$  is closer to the reference state  $X_{k,n}$  than a distance  $\epsilon_{k,n}$  in the window is computed as follows<sup>63</sup>:

$$P_{k,n}^{\epsilon_{k,n}} = \frac{1}{2(w_2 - w_1)} \sum_{\substack{m=1 \\ w_1 < |n-m| < w_2}}^N \mu_{k,n}(X_{k,m}) \quad (\text{A2})$$

For all,  $k$ ,  $\epsilon_{k,n}$  is obtained by making  $P_{k,n}^{\epsilon_{k,n}}$  equal to a small  $P_{ref} \ll 1$ . Through application of the Gaussian function to the states, values of the similarity of the states to the reference state are indicated through their Euclidean distances to the reference state. Standard deviations of the Gaussian functions are set equal to  $\epsilon_{k,n}$  and  $\epsilon_{r,n}$  for  $X_k$  and  $X_r$ , respectively. Centers of the Gaussian functions are the reference states ( $X_{k,n}$  and  $X_{r,n}$ ). Then, FSL between  $X_k$  and  $X_r$  restricted in the windows with centers  $X_{k,n}$  and  $X_{r,n}$ , respectively, is computed as follows<sup>63</sup>:

$$S_{k,n} = S_{r,n} = \frac{1}{2P_{ref}(w_2 - w_1)} \sum_{\substack{m=1 \\ w_1 < |n-m| < w_2}}^N [\mu_{k,n}(X_{k,m})\mu_{r,n}(X_{r,m})] \quad (A3)$$

Sliding the window over all the time series (shifting the window with a step), computing the FSL in each shifted window, and averaging the FSLs of all shifted windows lead to the FSL between the signals  $x_k$  and  $x_r$ .

### Declaration of Conflicting Interests

The author(s) declared no potential conflicts of interest with respect to the research, authorship, and/or publication of this article.

### Funding

The author(s) received no financial support for the research, authorship, and/or publication of this article.

### References

- Castellanos FX, Giedd JN, Eckburg P, et al. Quantitative morphology of the caudate nucleus in attention deficit hyperactivity disorder. *Am J Psychiatry*. 1994;151(12):1791–1796.
- Krain A, Castellanos FX. Brain development and ADHD. *Clin Psychol Rev*. 2006;26(4):433–444.
- Filipek PA, Semrud-Clikeman M, Steingard RJ, Renshaw PF, Kennedy DN, Biederman J. Volumetric MRI analysis comparing subjects having attention-deficit hyperactivity disorder with normal controls. *Neurology*. 1997;48(3):589–601.
- Qiu A, Crocetti D, Adler M, et al. Basal ganglia volume and shape in children with attention deficit hyperactivity disorder. *Am J Psychiatry*. 2009;166(1):74–82.
- Castellanos FX, Giedd JN, Marsh WL, et al. Quantitative brain magnetic resonance imaging in attention-deficit hyperactivity disorder. *Arch Gen Psychiatry*. 1996;53(7):607–616.
- Seidman LJ, Valera EM, Makris N. Structural brain imaging of attention-deficit/hyperactivity disorder. *Biol Psychiatry*. 2005;57(11):1263–1272.
- Mackie S, Shaw P, Lenroot R, et al. Cerebellar development and clinical outcome in attention deficit hyperactivity disorder. *Am J Psychiatry*. 2007;164(4):647–655.
- Plessen KJ, Bansal R, Zhu H, et al. Hippocampus and amygdala morphology in attention-deficit/hyperactivity disorder. *Arch Gen Psychiatry*. 2006;63(7):795–807.
- Aylward EH, Reiss AL, Reader MJ, Singer HS, Brown JE, Denckla MB. Basal ganglia volumes in children with attention-deficit hyperactivity disorder. *J Child Neurol*. 1996;11(2):112–115.
- Martins ALD, Mascarenhas NDA, Suazo CAT. *Spatio-temporal resolution enhancement of vocal tract MRI sequences based on image registration*, Integrated Computer-Aided Eng. 2011;18(2):143–156.
- Kramer MA, Chang FL, Cohen ME, Hudson D, Szeri AJ. Synchronization measures of the scalp EEG can discriminate healthy from Alzheimers subjects. *Int J Neural Syst*. 2007;17(2):61–69.
- Osterhage H, Mormann F, Wagner T, Lehnertz K. Measuring the directionality of coupling: phase versus state space dynamics and application to EEG time series. *Int J Neural Syst*. 2007;17(3):139–148.
- Lee H, Cichocki A, Choi S. Nonnegative matrix factorization for motor imagery EEG classification. *Int J Neural Syst*. 2007;17(4):305–317.
- Osorio I, Frei MG. Seizure abatement with single DC pulses: is phase resetting at play. *Int J Neural Syst*. 2009;19(3):149–156.
- Shoeb A, Gutttag J, Pang T, Schachter S. Non-invasive computerized system for automatically initiating vagus nerve stimulation following patient-specific detection of seizures or epileptiform discharges. *Int J Neural Syst*. 2009;19(3):157–172.
- Good LB, Sabesan S, Marsh ST, Tsakalis KS, Iasemidis LD. Control of synchronization of brain dynamics leads to control of epileptic seizures in rodents. *Int J Neural Syst*. 2009;19(3):173–196.
- Faust O, Acharya UR, Min LC, Spath BHC. Automatic identification of epileptic and background EEG signals using frequency domain parameters. *Int J Neural Syst*. 2010;20(2):159–176.
- Acharya R, Chua ECP, Chua KC, Min LC, Tamura T. Analysis and automatic identification of sleep stages using higher order spectra. *Int J Neural Syst*. 2010;20(6):509–521.
- Acharya UR, Vinitha Sree SV, Suri JS. Automatic detection of epileptic EEG signals using higher order cumulant features. *Int J Neural Syst*. 2011;21(5):403–414.
- Sherman D, Zhang N, Anderson M, et al. Detection of nonlinear interactions of EEG alpha waves in the brain by a new coherence measure and its application to epilepsy and anti-epileptic drug therapy. *Int J Neural Syst*. 2011;21(2):115–126.
- Hsu WY. Continuous EEG signal analysis for asynchronous BCI application. *Int J Neural Syst*. 2011;21(4):335–350.
- Ahmadlou A, Adeli H, Adeli A. Fractality and a wavelet-chaos methodology for EEG-based diagnosis of Alzheimer's disease. *Alzheimer Dis Assoc Disord*. 2011;25(1):85–92.
- Sankari Z, Adeli H. Probabilistic neural networks for EEG-based diagnosis of Alzheimer's disease using conventional and wavelet coherence. *J Neurosci Methods*. 2011;197(1):165–170.
- Sankari Z, Adeli H, Adeli A. Intrahemispheric, interhemispheric and distal EEG coherence in Alzheimer's disease. *Clin Neurophysiol*. 2011;122(5):897–906.
- Chakravarthy N, Sabesan S, Tsakalis K, Iasemidis L. Controlling synchronization in a neural-level population model. *Int J Neural Syst*. 2007;17(2):123–138.
- Chiappalone M, Vato A, Berdondini L, Koudelka M, Martinoia S. Network dynamics and synchronous activity in cultured cortical neurons. *Int J Neural Syst*. 2007;17(2):87–103.
- Postnov DE, Ryazanova LS, Zhirin RA, Mosekilde E, Sosnovtseva OV. Noise controlled synchronization in potassium coupled neural networks. *Int J Neural Syst*. 2007;17(2):105–113.

28. Chen M, Jiang CS, Wu QX, Chen WH. Synchronization in arrays of uncertain delay neural networks by decentralized feedback control. *Int J Neural Syst.* 2007;17(2):115–122.
29. Montina A, Mendoza C, Arecchi FT. Role of refractory period in homoclinic models of neural synchronization. *Int J Neural Syst.* 2007;17(2):79–86.
30. Neefs PJ, Steur E, Nijmeijer H. Network complexity and synchronous behaviour – an experimental approach. *Int J Neural Syst.* 2010;20(3):233–247.
31. Besio WG, Liu X, Wang L, Medvedev AV, Koka K. Transcutaneous focal electrical stimulation via concentric ring electrodes reduces synchrony induced by pentylentetrazole in beta and gamma bands in rats. *Int J Neural Syst.* 2011;21(2):139–149.
32. Lee L, Harrison LM, Mechelli A. A report of the functional connectivity workshop, Dusseldorf 2002. *Neuroimage.* 2003;19(2):457–465.
33. Jiang X, Adeli H. Fuzzy clustering approach for accurate embedding dimension identification in chaotic time series. *Integrated Computer-Aided Eng.* 2003;10(3):287–302.
34. Zou W, Chi Z, Lo KC. Improvement of image classification using wavelet coefficients with structured-based neural network. *Int J Neural Syst.* 2008;18(3):195–205.
35. Rizzi M, D'Aloia M, Castagnolo B. Computer aided detection of microcalcifications in digital mammograms adopting a wavelet decomposition. *Integrated Computer-Aided Eng.* 2009;16(2):91–103.
36. He Z, You X, Zhou L, Cheung Y, Tang YY. Writer identification using fractal dimension of wavelet subbands in gabor domain. *Integrated Computer-Aided Eng.* 2010;17(2):157–165.
37. Ghosh B, Basu B, O'Mahony M. Random process model for traffic flow using a wavelet-bayesian hierarchical technique. *Computer-Aided Civil and Infrastructure Eng.* 2010;25(8):613–624.
38. Ahmadlou M, Adeli H. Wavelet-synchronization methodology: a new approach for EEG-based diagnosis of ADHD. *Clin EEG Neurosci.* 2010;41(1):1–10.
39. Adeli H, Zhou Z, Dadmehr N. Analysis of EEG records in an epileptic patient using wavelet transform. *J Neurosci Methods.* 2003;123(1):69–87.
40. Adeli H, Ghosh-Dastidar S, Dadmehr N. A wavelet-chaos methodology for analysis of EEGs and EEG subbands to detect seizure and epilepsy. *IEEE Trans Biomed Eng.* 2007;54(2):205–211.
41. Ghosh-Dastidar S, Adeli H, Dadmehr N. Mixed-band wavelet-chaos-neural network methodology for epilepsy and epileptic seizure detection. *IEEE Trans Biomed Eng.* 2007;54(9):1545–1551.
42. Ghosh-Dastidar S, Adeli H. Spiking neural networks. *Int J Neural Syst.* 2009;19(4):295–308.
43. Ghosh-Dastidar S, Adeli H. A new supervised learning algorithm for multiple spiking neural networks with application in epilepsy and seizure detection. *Neural Netw.* 2009;22(10):1419–1431.
44. Ghosh-Dastidar S, Adeli H. Improved spiking neural networks for EEG classification and epilepsy and seizure detection. *Integrated Computer-Aided Eng.* 2007;14(3):187–212.
45. Ghosh-Dastidar S, Adeli H, Dadmehr N. Principal component analysis-enhanced cosine radial basis function neural network for robust epilepsy and seizure detection. *IEEE Trans Biomed Eng.* 2008;55(2):512–518.
46. Adeli H, Ghosh-Dastidar S. *Automated EEG-Based Diagnosis of Neurological Disorders-Inventing the Future of Neurology.* Taylor & Francis, Boca Raton, Florida: CRC Press; 2010.
47. Adeli H, Ghosh-Dastidar S, Dadmehr N. Alzheimer's disease and models of computation: imaging, classification, and neural models. *J Alzheimer's Dis.* 2005;7(3):187–199.
48. Adeli H, Ghosh-Dastidar S, Dadmehr N. Alzheimer's disease: models of computation and analysis of EEGs. *Clin EEG Neurosci.* 2005;36(3):131–140.
49. Adeli H, Ghosh-Dastidar S, Dadmehr N. A spatio-temporal wavelet-chaos methodology for EEG-based diagnosis of Alzheimer's disease. *Neuroscience Letters.* 2008;444(2):190–194.
50. Stam CJ, van Dijk BW. Synchronization likelihood: an unbiased measure of generalized synchronization in multivariate data sets. *Physica D: Nonlinear Phenomena.* 2002;163(3-4):236–251.
51. Watts DJ, Strogatz SH. Collective dynamics of 'small-world' networks. *Nature.* 1998;393(6684):409–410.
52. Sporns O, Zwi JD. The small world of the cerebral cortex. *Neuroinformatics.* 2004;2(2):145–162.
53. Bassett DS. Small-world brain networks. *Neuroscientist.* 2006;12(6):512–523.
54. Liu Y, Liang M, Zhou Y, et al. Disrupted small-world networks in schizophrenia. *Brain.* 2008;131(4):945–961.
55. Han FM, Wiercigroch M, Fang JA, Wang Z. Excitement and synchronization of small-world neuronal networks with short-term synaptic plasticity. *Int J Neural Syst.* 2011;21(5):415–525.
56. Gorban AN, Zinovyev A. Principal manifolds and graphs in practice: from molecular biology to dynamical systems. *Int J Neural Syst.* 2010;20(3):219–232.
57. Lattari L, Montenegro A, Conci A, et al. Using graph cuts in GPUs for color-based human skin segmentation. *Integrated Computer-Aided Eng.* 2011;18(1):41–59.
58. Faustino GM, Gattass M, de Lucena CJP, Campos PB, Rehen SK. A graph-mining algorithm for automatic detection and counting of embryonic stem cells in fluorescence microscopy image. *Integrated Computer-Aided Eng.* 2011;18(1):91–106.
59. Smit DJ, Stam CJ, Posthuma D, Boomsma DI, de Geus EJ. Heritability of "small-world" networks in the brain: a graph theoretical analysis of resting-state EEG functional connectivity. *Hum Brain Mapp.* 2008;29(12):1368–1378.
60. Bullmore E, Sporns O. Complex brain networks: graph theoretical analysis of structural and functional systems. *Nat Rev Neurosci.* 2009;10(3):186–198.
61. Stam CJ, Jones BF, Nolte G, Breakspear M, Scheltens P. Small-world networks and functional connectivity in Alzheimer's disease. *Cereb Cortex.* 2007;17(1):92–99.
62. Ahmadlou M, Adeli H. Fuzzy synchronization likelihood with application to attention deficit hyperactivity disorder. *Clin EEG Neurosci.* 2011;42(1):6–13.
63. Salvador R, Suckling J, Schwarzbauer C, Bullmore E. Undirected graphs of frequency-dependent functional connectivity in whole brain networks. *Philos Trans R Soc B: Biol Sci.* 2005;360(1457):937–946.



64. Ford JM, Mathalon DH. Neural synchrony in schizophrenia. *Schizophr Bull.* 2008;34(5):904–906.
65. Barrat A, Barthelemy M, Pastor-Satorras R, Vespignani A. The architecture of complex weighted networks. *Proc Natl Acad Sci U S A.* 2004;101(11):3747–3752.
66. Li W, Lin Y, Liu Y. The structure of weighted small-world networks. *Phys A: Stat Mech Appl.* 2007;376:708–718.
67. Latora V, Marchiori M. Economic small-world behavior in weighted networks. *European Phys J B-Condensed Matter and Complex Syst.* 2003;32(2):249–263.
68. Carmona S, Vilarroya O, Bielsa A, et al. Global and regional gray matter reductions in ADHD: a voxel-based morphometric study. *Neurosci Lett.* 2005;389(2):88–93.
69. Hale TS, McCracken JT, McGough JJ, Smalley SL, Phillips JM, Zaidel E. Impaired linguistic processing and atypical brain laterality in adults with ADHD. *Clin Neurosci Res.* 2005;5(5-6):255–263.
70. Chan KS, Tong H. *Chaos: A Statistical Perspective.* New York, NY: Springer; 2001:113–122.
71. Arnold J, Grassberger P, Lehnertz K, Elger CE. A robust method for detecting interdependences: application to intracranially recorded EEG. *Phys D: Nonlinear Phenomena.* 1999;134(4):419–430.
72. Pereda E, Rial R, Gamundi A, Gonzalez J. Assessment of changing interdependencies between human electroencephalograms using nonlinear methods. *Phys D: Nonlinear Phenomena.* 2001;148(1-2):147–158.